Journal Name

ARTICLE TYPE

Cite this: DOI: 00.0000/xxxxxxxxxx

Predicting Elemental Boiling Points from First Principles†

Jan-Michael Mewes*[a,b] and Odile R. Smits[b]

Received Date
Accepted Date

DOI: 00.0000/xxxxxxxxxx

The normal boiling point (NBP) is a fundamental property of liquids and marks the intersection of the Gibbs energies of the liquid and the gas phase at ambient pressure. This work provides the first comprehensive demonstration of the calculation of boiling points of atomic liquids through first-principles molecular-dynamics simulations. To this end, thermodynamic integration (TDI) and perturbation theory (TPT) are combined with a density-functional theory (DFT) Hamiltonian, which provides absolute Gibbs energies, internal energies, and entropies of atomic liquids with an accuracy of a few meV/atom. Linear extrapolation to the intersection with the Gibbs energy of a non-interacting gas phase eventually pins-down the NBPs. While these direct results can already be quite accurate, they are susceptible to a systematic over- or underbinding of the employed density functional. We show how the resulting errors can be strongly reduced by increasing the robustness of the method through a simple linear correction based on a high-level theoretical or experimental cohesive energy termed λ-scaling. By carefully tuning the technical parameters, the walltime per element could be reduced from weeks to about a day ($10-20$k core-hours), which enabled extensive testing for B, Al, Na, K, Ca, Sr, Ba, Mn, Cu, Xe and Hg. This comprehensive benchmark demonstrates the excellent performance and robustness of the approach with a mean absolute deviation (MAD) of less than 2% from experimental NBPs and very similar accuracy for liquid entropies (MAD 2.3 J/(mol*K), 2% relative). In some cases, the uncertainty in the predictions are several times smaller than the variation between literature values, allowing us to clear out ambiguities in the NBPs of B and Ba.

1 Introduction

The computational prediction and study of phase transitions is an active field of research.[1] The lion's share of this research focuses on transitions between condensed phases like melting or solid-solid transitions,[2–7] as these are most relevant for real-world applications as, *e.g.*, two polymorphs of the same substance can have significantly different properties. Perhaps because of this general focus, the prediction of NBPs from first-principle simulations is a sparsely populated field of research. The only other published study known to the author that demonstrates a calculation of NBPs largely based on a first-principles methodology is by Nakai and coworkers.[8] For this, they introduce the so-called harmonic solvation model (HSM) for calculating liquid Gibbs energies with a polarizable-continuum model (PCM). The HSM differs from the standard approach for thermochemical contributions in the treatment of translational and rotational degrees of freedom. In the HSM, they are replaced with additional vibrational modes resulting from freezing the PCM cavity in the frequency calculations. Comparing liquid Gibbs energies obtained with the HSM based on high-level CCSD(T) energies and an MP2 Hessian to Gibbs energies of the gas phase obtained with the standard ideal-gas model, they obtain very reasonable normal boiling points (NBPs) of 109.7°C and 66.9°C for water and ethanol, respectively. However, although the molecules themselves are described with a first-principles methodology, the description of intermolecular interactions in this approach is entirely based on a PCM with highly parametrized non-electrostatic contributions (SMD).[9] Most other approaches for the prediction of NBPs are entirely empirical data-driven methods that rely on machine-learning and quantitative structure-property relationships (QSPR).[10–12] As such, they can often be related to the group-contribution method of Joback and Reid.[13] Although some of these protocols make use of first-principles calculations to refine the predictions,[11] there have been no attempts based solely on first-principles methods.

In general, the calculation of phase-transition temperatures through computer simulations can be carried out in two ways: (i) So-called direct approaches attempt to simulate the phase transition either in time (*e.g.* void method or cluster melting),[14,15] or in space (*e.g.* interface pinning).[7] Such direct approaches are complicated by super-heating and super-cooling. As a result, all the methods mentioned above are attempts to avoid,

[a] *Mulliken Center for Theoretical Chemistry, University of Bonn, Beringstr. 4, 53115 Bonn, Germany, janmewes@janmewes.de*
[b] *Centre for Theoretical Chemistry and Physics, The New Zealand Institute for Advanced Study, Massey University Auckland, 0632 Auckland, New Zealand*

† Electronic Supplementary Information (ESI) available: [details of any supplementary information available should be included here]. See DOI: 00.0000/00000000.

mitigate, or minimize these phenomena. (ii) So-called indirect approaches circumvent these problems through calculating Gibbs energies (also Gibbs free energies and thus free-energy methods) of the respective phases separately, and subsequently, locate the point of intersection, *i.e.*, where $\Delta G = 0$. This not only eliminates the problems with super-heating and cooling, but allows to exploit these phenomena to achieve faster equilibration, *e.g.*, in solid simulations well above the melting point,[16] or here in liquid simulations above the boiling point. Gibbs-energy based approaches may be further divided into two groups: On the one hand, there are approaches based on relative Gibbs energies (iia) (*e.g.* the pseudo-supercritical path method)[17], and on the other, there are approaches which attempt the calculation of absolute Gibbs energies (iib). For a more detailed overview and discussion of these approaches, the interested reader is referred to refs. 18 and 6. Specifically concerning boiling points, direct approaches (i) as well as those focusing on Gibbs-energy differences (iia) are problematic due to the drastic differences between the condensed and gaseous phases in terms of volume. Hence, we approach the problem by calculating absolute Gibbs energies.

One approach for the calculation of absolute Gibbs energies of liquids was recently presented by Kresse and coworkers,[19] and employed to study the melting of silicon and magnesia (MgO).[19,20] We have further developed this approach to include spin-orbit relativistic effects to explore the physicochemical properties and aggregation state of the super-heavy element Cn.[16] Since Cn has been inferred to be highly volatile,[21] it was necessary to include the NBP. For this purpose, the herein presented concept was developed. This work describes the adaptation of and a correction to this approach to efficiently calculate NBPs, as well as the comprehensive testing for a representative set of elements, including insulators, semiconductors, and metals.

An important aspect of the approach and this work is a correction of the calculated transition temperatures based on the ratio between the cohesive (also atomization) energy calculated at the same level as the Gibbs energy (here DFT), and a high-level reference or experimental value, *i.e.*, $\lambda = E_{\mathrm{coh}}^{\mathrm{ref}}/E_{\mathrm{coh}}^{\mathrm{DFT}}$. Due to this definition, linearly scaling the DFT Hamiltonian with λ matches the overall interaction strength of DFT to that of the high-level reference. Since this so-called λ-scaling systematically reduces any strong over- or underbinding of the chosen density-functional approximation (DFA), it increases the accuracy and in particular the robustness of the approach concerning the choice of the functional. While the article introducing this correction makes use of a high-level theoretical CCSD(T) reference,[16] this work mostly employs experimental references since such high-level calculations are not readily available for all elements considered here. Although this introduces a certain degree of empiricism, we argue that very similar results would be obtained by using high-level theoretical values, as is demonstrated for Xe.

Before we move to the main article, it bears pointing out that to our surprise, we found the literature to be peppered with conflicting values for the NBPs of common elements, *e.g.*, K (1.5% variation), B (8.7% variation) and Ba (17% variation). This and related uncertainties have been studied in detail by Zhang and coworkers,[22] who employed neural networks to rectify conflicts between several major reference books.[23–27] Exploiting, *e.g.*, the relation between the enthalpy of evaporation and the NBP, they eventually suggested the most probable and consistent values. We will follow their suggestions in this work, which are consistent with our calculations in all but one example. In addition to the sources considered by Zhang and coworkers, we also include values from the prominent Hollemann-Wiberg.[28]

2 Approach

The normal boiling point (NBP) is defined as the intersection of the Gibbs energies

$$G(T,p) = U(T) + pV - TS(T) \tag{1}$$

of the liquid and gas phase at their respective equilibrium volume at normal pressure (1013 mBar). To locate this point, the gas phase is modelled analytically using the ideal-gas law (eq. 11 in the SI)[†], while G^l is calculated through thermodynamic integration (TDI) at a given simulation temperature T_{sim}, at its equilibrium volume (calculation described in the SI)[†], in the classical Born-Oppenheimer approximation. Since we use the liquid equilibrium volume, we assume $pV = 0$, and thus $H^l = U^l$ to simplify the problem. This is possible since the pV term for liquids at ambient pressure is entirely negligible ($\ll 1$ meV/atom, e.g. 0.06 meV/atom for K with the largest atomic volume). For the gas-phase, the pV term is substantial (e.g. 86.2 meV/atom for K at 1000 K and 1013 mBar) and thus included in G^g. The reference for the TDI is the analytically known non-interacting gas at the liquid volume (with the internal energy U_0 and Gibbs energy G_0 from eq. 11 in the SI).[†] Accordingly, integration along the interaction strength λ, which relates the interacting (DFT) liquid (with U_1 and G_1) with the non-interacting reference

$$G_1 = G_0 + \Delta G_{0-1} = G_0 + \int_0^1 d\lambda \langle U_1(\mathbf{R}) - U_0(\mathbf{R}) \rangle_\lambda \,, \tag{2}$$

provides the Gibbs-energy difference between the ideal reference and the DFT liquid ΔG_{0-1}. TDI is followed by several steps of thermodynamic perturbation theory (TPT) as detailed in the SI[†] to achieve high numerical precision in terms of plane-wave cut-offs and k-point convergence, as well as to include spin-orbit coupling (SOC). Adding these contributions to G_1 provides the final G^l. All calculations for the liquid are conducted for 64-atom configurations (Xe: 61) since previous studies have shown this number to provide converged Gibbs energies compared to larger cells with > 200 atoms.[16,19,20]

The central challenge of this approach is to accurately evaluate the integral in eq. (2), which typically provides a large part of G^l. This is accomplished by numerical integration using an n point Gauss-Lobatto rule. For this purpose, the integral has to be transformed to adapt the limits from $[0,1]$ to $[-1,1]$, which yields (details in the SI)[†]

$$\Delta G_{0-1} = \frac{1}{2(1-\kappa)} \int_{-1}^{1} f(\lambda(x))\lambda(x)^\kappa dx \,. \tag{3}$$

To avoid a singularity at $\lambda = 0$, the parameter $\kappa = [0 \ldots 1[$ is introduced, which also allows to guide the placement of the quadra-

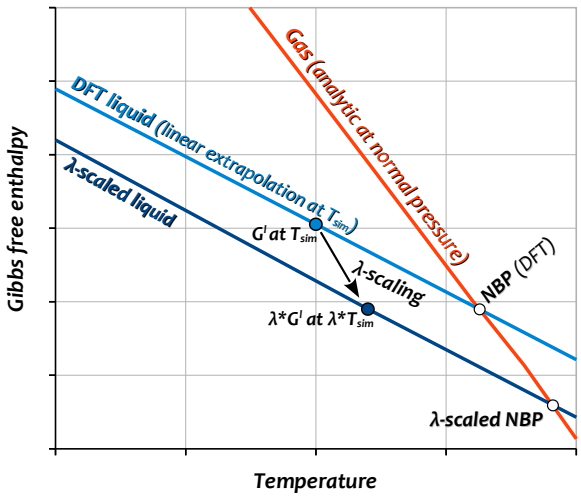

Fig. 1 Schematic demonstration of the approach to calculate NBPs as the intersection of the analytic Gibbs energy of the (ideal) gas with that of the liquid at the DFT level (light blue, provides direct NBP) and corrected *via* λ-scaling (dark blue, provides corrected NBP). The plot shows the effect of $\lambda = 1.1$, corresponding to a significant underbinding of the DFT Hamiltonian.

ture points. The closer κ is to one, the more the points are moved towards the non-interacting limit (small λ), while $\kappa = 0$ would retain the equidistant spacing of the Gauss-Lobatto rule. A detailed explanation and visualization of this rather technical aspect is provided in the SI.[†] The important part to recognize is that κ and n govern the balance between accuracy and computational effort. The higher n, the more simulations have to be conducted, and the higher κ, the smaller are the λ values and thus interatomic forces in these simulations. Depending to some extend on the system, such simulations with small forces become increasingly unstable and tedious at $\lambda < 0.01$. As this strongly increases the demands in human and computer time, it is a central task of this work to find values for κ and n that provide a good balance between accuracy of the integration and computational cost. Having obtained G^l at T_{sim}, the temperature-dependence due to the liquid entropy is approximated linearly, *i.e.*, $S^l = (U^l - G^l)/T_{\mathrm{sim}}$, where U^l is the average of kinetic and potential energy from a canonical (NVT) MD simulation ($\lambda = 1$). This enables extrapolation to the intersection with the Gibbs energy of the gas phase G^g as illustrated in Fig. 1, providing the NBP.

To address any systematic over- or underbinding of the employed DFA, the results are corrected using λ-scaling. To rationalize this correction, it is instructive to consider how it was initially conceived: As an adaptation of upper limit of the integral over the interaction strength λ in eq. (2). Since λ is intended as a linear correction for the DFT Hamiltonian, it is defined as the ratio between the cohesive (atomization) energy of (here) DFT divided by the high-level reference ($E_{\mathrm{coh}}^{\mathrm{ref}}/E_{\mathrm{coh}}^{\mathrm{DFT}}$). Thus, by replacing the upper limit of the integral with λ, it is ensured that the integration based on the DFT Hamiltonian spans the same range of interaction strength as provided by the high-level reference. It is important to recognize that while this correction largely eliminates any systematic differences between DFT and the high-level reference such as over- or underbinding (potential dept), it does not correct for deviations in the shape of the inter-atomic potentials (narrowness, asymptotic behavior, etc.).

However, instead of changing the integration limits for every single case, it is more convenient to use an *a posteriori* correction of the G^l calculated at the DFT level illustrated in Fig. 1. Already during the first application of the λ-scaling,[16] it was recognized and eventually proved that for any phase transition (between condensed phases) in the classical Born-Oppenheimer picture, λ-scaling is formally equivalent to simply multiplying the (transition) temperature with λ.[16] This is because scaling both potential and (simulation) temperature by the same factor cancels out, such that on average the same configurations are generated (S remains the same, U scales with λ, *cf.* eqs. 3-5). However, when considering transitions involving the gas phase, the potential (entering only *via* the tiny virial two-body correction) hardly matters, such that the gas-phase essentially remains unaltered in Fig. 1, and in turn the simple transition-temperature becomes invalid (the results are only a few percent off, and thus the formally wrong scaling for the BP went undetected in ref. 16). Here we use the following relations for the liquid phase (proof in the SI)[†]

$$\lambda U(T,\phi) = U(\lambda T, \lambda \phi) \tag{4}$$

$$S(T,\phi) = S(\lambda T, \lambda \phi) \text{ and thus} \tag{5}$$

$$\lambda G(T,\phi) = G(\lambda T, \lambda \phi)\,, \tag{6}$$

to scale the Gibbs energy of the liquid calculated at the DFT level (light blue line in Fig. 1) to obtain a corrected G^l (dark blue line in Fig. 1). For this, G^l calculated at the simulation temperature T with the (unscaled) DFT potential (ϕ) is multiplied with λ, which provides a corrected Gibbs energy (approximating the high-level Hamiltonian $\lambda\phi$) at the effective temperature (λT). The λ-scaled NBP is thus obtained as the intersection between the corrected G^l and the (unaltered) Gibbs energy of the gas phase *via* linear extrapolation. Along the same lines of thought, λ-scaling can not only be seen as a correction in the potential, but also as a correction of the temperature. Assuming, e.g., that the employed DFT potential is twice as deep as the reference potential and thus $\lambda = 0.5$, the configurations generated by a DFT-MD simulation with $\lambda = 1$ correspond to those obtained with the reference Hamiltonian at $0.5 * T_{\mathrm{sim}}$.

For the metallic liquids considered here, an additional complication arises through the electronic entropy S_{el}, which is significant at elevated temperature of the NBP (up to 10% of the total S, *cf.* Tab. 6 in SI)[†], but is not included in the classical S. To address this consistently, we include S_{el} in the internal energy through Fermi-smearing of the orbital populations,[29] which corresponds to neglecting the non-classical temperature dependence of G. Exploratory calculations have shown that this only leads to small changes of a few K in the calculated NBPs and is thus acceptable. However, when comparing the calculated liquid entropies to experimental references, including S_{el} in S distinctly improves the agreement (*cf.* Fig. 3).

3 Results and Discussion

3.1 Detailed Considerations for Xe, K and B

We begin the discussion with a detailed look at Xe, K, and B to establish the capabilities and limitations of the approach for a small but diverse group of elements. In contrast to all other systems considered here, Xe atoms are weakly interacting, and their bulk forms an insulator, like most noble-gas solids.[30] As a result of their weakly interacting nature, noble-gas liquids are often considered as prototypical Lennard-Jones fluids. Although this suggests that an atom-pairwise potential may be suitable, it has recently been shown that the melting point of Xe deviates from the experiment by as much as 20 K if three-body effects are omitted.[31] We employ the PBE and revPBE density-functional approximations (DFAs),[32–34] both of which are combined with Grimme's atom-pairwise D3 correction with the default Becke-Johnson damping (in the following just D3).[35,36] Hence, three-body effects are only taken into account in the DFT part of the calculation. Nevertheless, PBE-D3 accurately recovers the experimental cohesive energy of -0.164 eV of solid *fcc* Xe. Accordingly, the scaling factor $\lambda = E_{\mathrm{coh}}^{\mathrm{exp}}/E_{\mathrm{coh}}^{\mathrm{calc}}$ is unity. In contrast, revPBE-D3 overbinds slightly with -0.191 eV, resulting in a λ of 0.859.

We calculated Gibbs energies of liquid Xe at the experimental NBP of 165 K with both DFAs. With PBE-D3, we moreover explore the parameters for the integration, as well as increasing the simulation temperature T_{sim} to 200 K. The results of these calculations are compiled in Tab. 2, while a breakdown of the liquid Gibbs energy is provided in Tab. 1. Inspection shows that in particular the calculations with PBE-D3 are in excellent agreement with the experimental NBP of Xe of 165 K. The results are moreover virtually identical for both simulation temperatures, and there is excellent agreement between the entropy-based linear extrapolation at each T_{sim} with a direct interpolation between the Gibbs energies calculated at 165 K and 200 K. The overbinding of revPBE-D3 evident from $\lambda < 1$ causes the liquid to be too stable and, in turn, the calculated NBP to be too high by 30 K. However, this systematic deviation is strongly reduced through λ-scaling. To eliminate the empiricism introduced by this scaling, the experimental cohesive energy in the calculation of λ can be replaced with a high-level theoretical value of -0.166 eV, which has been derived from coupled-cluster calculations and includes zero-point vibrational energies (ZPVE).[37] This results in a slight change of the λs to 1.017 (PBE-D3) and 0.874 (revPBE-D3), and, accordingly, also the calculated NBPs are very similar ranging from $169-177$ K.

This brings us to another aspect, namely the influence of ZPVE, which is relatively large for Xe due to its small cohesive energy. Using the ZPVE-uncorrected high-level value from ref. 37 of 0.172 eV (or back-correcting the experimental value) distinctly increases the λs to 1.053 (PBE-D3) and 0.905 (revPBE-D3), and significantly worsens the agreement with the experiment as evident from the NBPs of 176-181 K. This suggests that implicitly including ZPVE *via* the cohesive energy corrects for the absence of ZPE in our otherwise entirely classical approach. Thus, we will use ZPVE-uncorrected λs in the following. In any case, the relative size of the ZPVE is distinctly smaller in all further examples (*cf.* Tab. III in ref. 38).

Potassium is a metallic liquid with a NBP of 1047 K[23–25] as suggested by Zhang and coworkers,[22] while other sources give values of 1026 K,[28] 1032 K,[26,27] and 1040 K.[39] Although gaseous K atoms exhibit a strong pairwise interaction in the form of a covalent bond of 0.55 eV, the resulting virial correction (eq. (13) in SI with $\sigma = 3.496$ Å and $\varepsilon = 0.55$ eV)[†] merely amounts to 1.2 meV/atom at 1000 K, and thus hardly affects the NBP ($\Delta T \approx 1$ K). Another result of this strong interaction is that potassium vapor is known to consist of about 5% dimers at the NBP.[39,40] However, exploring the impact of dimerization using the Quantum-Cluster Equilibrium (QCE) approach as implemented in the Peacemaker program[41,42] revealed that this has negligible influence on the Gibbs energy at 1000 K (< 1 meV). The reason is that the decrease in entropy just cancels the stabilizing effects on internal energy and volume (pV). For reference, the electronic double-degeneracy ($\Theta = 2$) of K atoms stabilizes the gas by about 60 meV, decreasing the BP by about 75 K.

Solid K crystallizes in a body-centred cubic (*bcc*) lattice, for which PBEsol provides excellent agreement with the experimental cohesive energy ($\lambda = 1.002$). We will thus use PBEsol in most calculations, and conduct additional tests with PBE and the dispersion-corrected PBE-D3. To test the consistency of the extrapolation scheme for this metallic system, we conducted Gibbs-

Table 1 Breakdown of the contributions to the Gibbs energy for the liquids of Xe, K, and B from TDI and TPT at the simulation temperature as well as the influence of λ-scaling. Following the element, the employed DFA and corresponding λ, simulation temperature T_{sim} and density ρ are given. The column ΔG provides the contribution of each step, while "total G" is the running sum. Θ is the electronic degeneracy of the atoms in the gas phase. The last row provides the Gibbs energy of the gas phase at the simulation temperature. A table with the final values for all studied elements is provided in the SI.[†] All values are given in eV/atom.

step, cut-off, k-grid	ΔG	total G	U	TS
Xenon, PBE-D3 ($\lambda = 1.0003$), 165 K, $\rho = 2.73$ g/ccm				
non-interacting		-0.1657	0.0213	0.1870
TDI, 150, Γ	-0.0775	-0.2432	-0.1470	0.0962
TPT, 300, Γ	0.0065	-0.2367	-0.1405	0.0962
TPT, 300, 2^3	-0.0001	-0.2368	-0.1406	0.0962
λ-scaled	0.0000	-0.2368	-0.1406	0.0962
gas phase, $\Theta = 1$		-0.2334	0.0213	0.2547
Potassium, PBEsol ($\lambda = 1.002$), 1000 K, $\rho = 0.696$ g/ccm				
non-interacting		-1.1004	0.1293	1.2297
TDI, 250, Γ	-0.6329	-1.7332	-0.6392	1.1128
TPT, 500, Γ	-0.0003	-1.7335	-0.6397	1.1128
TPT, 500, 2^3	0.0024	-1.7311	-0.6371	1.1128
λ-scaled	-0.0010	-1.7321	-0.6381	1.1150
gas phase, $\Theta = 2$		-1.7076	0.1293	1.8369
Boron, PBE-D3 ($\lambda = 0.916$), 4000 K, $\rho = 2.04$ g/ccm				
non-interacting		-3.6408	0.5170	4.1578
TDI, 350, 2^3	-4.8897	-8.5305	-4.8311	3.7015
TPT, 600, 2^3	-0.0072	-8.5378	-4.8383	3.7015
TPT, 600, 3^3	0.0009	-8.5368	-4.8373	3.7015
λ-scaled	0.4063	-8.1305	-4.3310	3.3906
gas phase, $\Theta = 6$		-7.7326	0.5170	8.2496

Table 2 Calculated and experimental normal boiling points (NBPs) of Xe, K and B. Experimental data taken from Holleman-Wiberg as well as from Zhang and coworkers with their suggestions set in bold.[22,28] Calculated data is given for various DFAs, T_{sim}, integration parameters (κ and n), pressures, as well as with and without λ-scaling. "A//B" indicates that TPT was used to calculate the Gibbs energy with method A for configurations obtained with method B. The reference cohesive energy and lattice used in the calculations used to determine λ is given in eV/atom after the name of the respective element.[43] For Xe and K, we also provide NBPs obtained by interpolation between the calculations at 165 K and 200 K (Xe), and 923 K, 1023 K, and 1123 K (K).

		NBP /K	
DFA, T_{sim}, n, κ	λ	direct	λ-scaled
Xenon, $E_{\mathrm{coh}}^{\mathrm{exp}} = -0.164$ (*fcc*)		lit. **165.2** K	
PBE-D3, 165, 7, 0.75	1.000	166.9	166.9
PBE-D3, 200, 7, 0.75	1.000	166.5	166.5
PBE-D3, *interpolated*,	1.000	166.7	166.6
revPBE-D3, 165, 8, 0.60	0.859	195.2	174.3
Potassium, $E_{\mathrm{coh}}^{\mathrm{exp}} = -0.934$ (*bcc*)		lit. 1026, 1032, **1047** K	
PBEsol, 1023, 7, 0.60	1.002	1028	1030
PBEsol, 1023, 7, 0.70	1.002	1027	1029
PBEsol, 1023, 7, 0.75	1.002	1028	1030
PBEsol, 923, 7, 0.75	1.002	1027	1029
PBEsol, 1123, 7, 0.75	1.002	1029	1031
PBEsol, *interpolated*	1.002	1030	1030
PBEsol, 1023, vol−	1.002	1027	1030
PBEsol, 1023, vol+	1.002	1028	1030
PBE, 1000, 7, 0.60	1.073	968.5	1020
PBE-D3, 1000, 7, 0.60	0.945	1064	1022
PBEsol, 1000, 7, 0.60	1.002	1029	1030
PBEsol//PBE-D3, 1000	1.002	1026	1028
Boron, $E_{\mathrm{coh}}^{\mathrm{exp}} = -5.920$ (α-B)		lit. 3931, **4203**, 4273 K	
PBE-D3, 4000, 6, 0.60	0.916	4643	4317
PBE-D3, 4000, 8, 0.60	0.916	4645	4320
PBE-D3, 4000, 10, 0.60	0.916	4649	4323
PBE//PBE-D3, 4000	0.928	4505	4233
SCAN//PBE-D3, 4000	0.932	4433	4183
SCAN-rVV10//PBE-D3, 4000	0.921	4433	4197

energy calculations for liquid K at temperatures of 923 K (650°C), 1000 K, 1023 K (750°C) and 1123 K (850°C). For the calculations at 1023 K, we tested three different values for κ (0.75, 0.70 and 0.60). Finally, to establish the sensitivity concerning the employed volume, we conducted additional calculations at 1023 K with the cell-dimensions varied by ±2%, corresponding to $\Delta V \approx 6\%$ and $\langle p \rangle = 0.8/-0.5$ kBar.

The results for K are compiled in Tab. 2, while a detailed breakdown of the contributions to the Gibbs energy for the PBEsol calculation at 1000 K is provided in Tab. 1. Inspection shows that first and foremost, all results obtained with PBEsol are consistent and virtually independent of the tested parameters. Interpolation between the Gibbs energies calculated with PBEsol at 923 K, 1023 K, and 1123 K provides virtually the same NBP as the entropy-based extrapolation. Since the calculations at different volumes yield such consistent NBPs it is questionable if the differences are significant considering the statistical uncertainties of 1-2 K. Also, the parameters for the numerical integration do not exert any significant influence in the calculated NBP, showing that $\kappa = 0.6$ is sufficiently accurate. Compared to PBEsol, PBE-D3 slightly overbinds solid K as evident from $\lambda = 0.945$, whereas plain PBE slightly underbinds ($\lambda = 1.073$). The direct (unscaled) results for the NBP are as one would expect: The overbinding PBE-D3 stabilizes the liquid over the gas phase, moving the calculated NBP to higher temperatures (1064 K), while the underbinding PBE provides a lower NBP of 969 K. Similar to Xe, λ-scaling strongly reduces the deviation. Finally, to demonstrate TPT between DFAs, we recalculate 10 configurations from the PBE-D3 simulation with PBEsol. The resulting correction of G^l of 33.3 meV moves the NBP to 1028 K, and thus very close to the consistent PBEsol result. Altogether, our predictions favor the lower literature values for the NBP of K of $1026-1032$ K, in agreement with the CRC Handbook and the Tables of Physical and Chemical Constants (better known as "Kaye and Laby"),[26,27] whereas the value of 1047 K suggested by Zhang and coworkers (without any discussion of data to support it) appears too high at first glance. However, the deviation of the two values is only about 1.5%, and thus just below the statistical accuracy of our method.

Bulk boron is a covalently bound semiconductor. The literature values of its NBP vary widely from 3931 K[25,28] over 4203 K[23,24] to 4273 K.[26,27] The gas phase consists of isolated boron atoms with $\Theta = 6$. To determine the scaling factor λ, we employ α-rhombohedral boron (12 atoms/unit cell) instead of the thermodynamically most stable β-rhombohedral phase (105-108 atoms/unit-cell)[44] to avoid dealing with partial occupations. Since the energy difference between the two phases is very small,[44] this should not lead to any significant differences. For α-boron, PBE, PBE-D3 and SCAN provide good agreement with the experimental cohesive energy as evident from the respective λs of 0.928, 0.919 and 0.932. We calculate the Gibbs energy at 4000 K with PBE-D3 and subsequently use TPT to include also SCAN, SCAN-rVV10 and plain PBE. To elucidate the influence of the number of quadrature points on the accuracy of the NBP, we conducted the numerical integration for B with 6, 8, and 10 points. Since increasing the number of points includes calculations for increasingly small λ values of 0.0047 (6 points), 0.0010 (8 points) and 0.0003 (10 points), this improves the sampling of the at 4000 K particularly important repulsive part of the configuration space (*cf.* Fig. 4 in SI)[†]. However, there is only small decrease of the value of the integral by ≈ 3 meV/atom from 6 to 8 points, and again by the same amount from 8 to 10 points. Although these deviations are an order of magnitude larger than the statistical error, they translate to a total ΔT of merely 6 K (6 to 10 points), or 0.1% of the NBP. The NBPs calculated with other DFAs range from 4183 K (SCAN) over 4233 K (PBE) to 4323 K (PBE-D3). They are all in good agreement with the experimental value of 4203 K suggested by Zhang and coworkers (3% deviation for PBE-D3, $< 1\%$ for PBE, SCAN, and SCAN-rVV10),[22] as well as with the value of 4273 K from refs. 26 and 27. In contrast, the value of 3931 K reported in refs. 25 and 28 is too low by $6-10\%$. This is more than twice the mean absolute deviation (MAD) over all studied elements, and the value thus presumably wrong.

To summarize, the two most relevant results from this detailed look at Xe, K and B are (i) the approach is robust concerning simulation temperature, volume, and also concerning the choice of

the density functional, and (ii) TDI conducted with 6-8 quadrature points and $\kappa = 0.60$ is sufficiently accurate for the determination of NBPs. This last point is of particular practical relevance since these settings lead to much more stable and efficient simulations compared to the previously used settings. This allowed us to test the approach for many more elements, which we will discuss in the following.

3.2 Additional Elements

We conducted additional calculations for sodium (Na), aluminum (Al), calcium (Ca), strontium (Sr), barium (Ba), manganese (Mn), copper (Cu), and mercury (Hg). Their gas phases consist of isolated atoms with $\Theta = 1$ (Ca, Sr, Ba, Hg), 2 (Na, Cu) or 6 (Al, Mn). Cu and Ba moreover exhibit low-lying electronically excited states which are significantly populated near their NBPs. This causes a stabilization of the gas phase by 23 meV/atom for Cu and 32 meV/atom for Ba at the NBP (energy differences relative to ref. 39), which in turn significantly affects the calculated NBP. We take this into account pragmatically, *i.e.*, by using fractional degeneracies of 2.19 and 1.18 for Cu and Ba, which quantitatively restores the agreement with the reference values at and around the NBP. A notable interaction between the atoms in the gas phase exists only in case of Na ($\varepsilon = 0.75$ eV, $\sigma = 2.76$ Å),[45] Al ($\varepsilon = 1.66$ eV, $\sigma = 2.41$ Å),[46] and Cu ($\varepsilon = 2.03$ eV, $\sigma = 1.98$ Å).[47] However, similar to K, neither of these experience a significant contribution from the two-body term at the NBP (Na −0.79 meV, Al −0.49 meV, Cu −0.37 meV). The gas phases of Na and possibly also Al and Cu may contain some dimers, but as already discussed their influence on the Gibbs energy is negligible at the NBP.

For Na, Al, Ca, Sr, Cu, and Hg, the variation between the experimental references is small, and the agreement with the calculated NBPs very good, as evident from Fig. 2 and Tab. 3. The mean absolute deviation (MAD) over all elements with respect to the literature values suggested by Zhang and coworkers is just 1.62% and the mean deviation (MD) −0.80% (PBE for the alkaline-earth, transition metals, B and Al, PBEsol for K and Na, PBE-D3 for and Xe). The results further demonstrate how λ-scaling improves the predicted NBP, in particular, if there exists significant over- or underbinding at the DFT level, *i.e.*, when λ deviates from unity (*cf.* B, Ca, Sr, Mn, Hg). As a result, the final λ-scaled NBPs calculated with various DFAs are consistent despite substantial differences in the DFA description of the respective bulk solids (*cf.* PBE/PBE-D3/PBEsol for the alkaline-earth metals). For Na, we included a Gibbs energy calculated at a simulation temperature of just 400 K, *i.e.*, just above the melting point as a hardship case for the entropy-based extrapolation. Despite the large ΔT, the resulting NBP is very reasonable with 1022 K, and constitutes an ideal starting point for a more accurate calculation.

Mn and Ba stand out from the other results. For Mn, the variation in the experimental NBP is not too large with a range of 2235 – 2373 K (6%),[22] whereas the variation between the calculated NBPs is unusually large. We first employed RPBE and subsequently also SCAN because they provide a much better agreement for the cohesive energy of α-Mn (distorted *bcc* with 51 atoms/cell) than PBE, as evident from the respective λs of 0.916

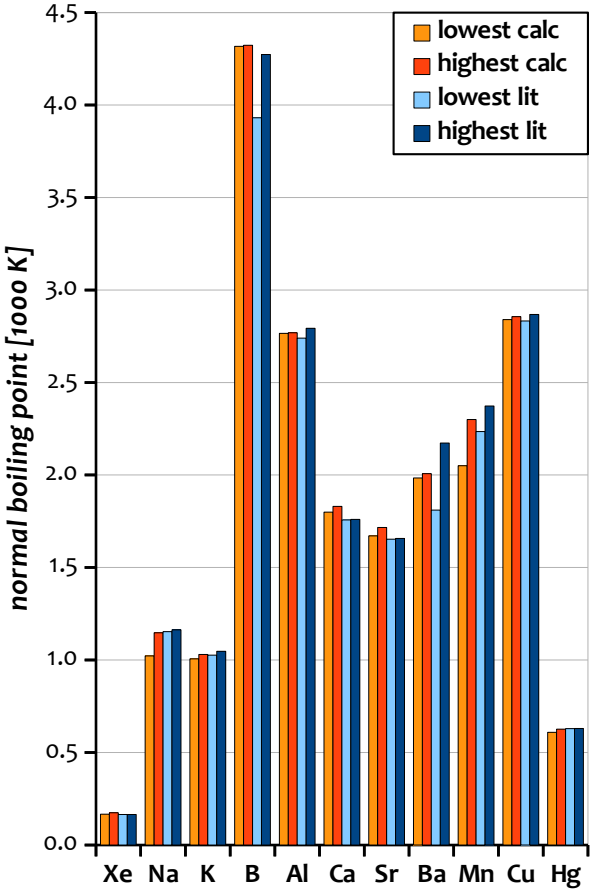

Fig. 2 Plot of the range of calculated values (orange and red, all λ-scaled) against the range of literature values (light and dark blue) as shown in Tabs. 2 and 3. The MAD over all elements with respect to the literature values suggested by Zhang and coworkers is just 1.62% and the MD −0.80% (based on the PBE for the alkaline-earth, transition metals, B and Al, PBEsol for K and Na, PBE-D3 for and Xe).

(RPBE), 0.980 (SCAN), and 0.751 (PBE). This strong overbinding is particularly surprising since PBE tends to underbinding for all other elements considered here and in general.[38] However, despite their good agreement for the cohesive energy, the NBPs calculated with RPBE and, in particular, with SCAN fall significantly short of the range of experimental values with relative deviations of 4% and 8% (with respect to the lower value of 2235 K). Surprisingly, the calculation with PBE (conducted at an increased temperature of 3200 K to bring the effective temperature closer to the NBP) provides an NBP of 2300 K and thus in between the experimental values. Although further calculations would be required to draw any final conclusions, these results suggest the good agreement of RPBE and SCAN for the cohesive energy is the result of a fortuitous error compensation between the energy of the bulk and the energy of the isolated atom. Despite its stark overbinding of the solid, PBE appears to provide a more consistent description of the solid and liquid, such that our approach predicts a more reasonable NBP. We speculate that these issues are the result of the challenging electronic structure of this *d*-block element with several partially occupied shells. This may impact the calculation of the isolated atom as well as the

Table 3 Calculated and experimental NBPs for the second set of elements. Experimental data taken from Holleman-Wiberg as well as from Zhang and coworkers with their suggestions set in bold.[22,28] Calculated data is given for various DFAs, T_{sim}s, as well as with and without λ-scaling. All calculations are conducted in the scalar-relativistic approximation except for Ba and Hg, for which (also) spin-orbit (so) relativistic results (*via* TPT) are presented.

		NBP /K	
DFA, T_{sim}, n, κ	λ	direct	λ-scaled
Sodium, $E_{\mathrm{coh}}^{\mathrm{exp}} = -1.113$ (*bcc*)		lit. 1153−**1163** K	
PBEsol, 1000, 7, 0.60	0.958	1184	1147
PBEsol, 400, 7, 0.70	0.958	1043	1022
Aluminum, $E_{\mathrm{coh}}^{\mathrm{exp}} = -3.390$ (*fcc*)		lit. **2743**−2793 K	
PBE, 2800, 7, 0.60	0.994	2783	2769
Calcium, $E_{\mathrm{coh}}^{\mathrm{exp}} = -1.840$ (*fcc*)		lit. 1757−**1760** K	
PBE, 1800, 7, 0.60	0.961	1854	1799
PBE-D3, 1800, 6, 0.60	0.855	2050	1815
PBEsol, 1800, 8, 0.60	0.871	2037	1830
Strontium, $E_{\mathrm{coh}}^{\mathrm{exp}} = -1.720$ (*fcc*)		lit. **1653**−1657 K	
PBE, 1570, 7, 0.50	1.071	1586	1671
PBE-D3, 1800, 7, 0.60	0.951	1775	1708
PBEsol, 1800, 7, 0.60	0.952	1781	1716
Barium, $E_{\mathrm{coh}}^{\mathrm{exp}} = -1.720$ (*bcc*)		lit. 1810,[28] **1910**−2173 K	
PBE, 2000, 7, 0.60	1.013	1966	1987
soPBE, 2000, 7, 0.60	1.010	1970	1984
PBE-D3, 2000, 7, 0.60	0.915	2144	2007
Mangan, $E_{\mathrm{coh}}^{\mathrm{exp}} = -2.920$ (α-*Mn*)		lit. 2235−**2373** K	
PBE, 3200, 7, 0.60	0.751	2924	2300
RPBE, 2400, 8, 0.60	0.916	2309	2144
SCAN, 2400, 8, 0.60	0.980	2082	2050
Copper, $E_{\mathrm{coh}}^{\mathrm{exp}} = -3.490$ (*fcc*)		lit. 2833−**2868** K	
PBE, 2700, 7, 0.60	1.002	2836	2840
PBE, 3000, 7, 0.60	1.002	2851	2856
Mercury, $E_{\mathrm{coh}}^{\mathrm{exp}} = -0.670$ (*rho*)		lit. 629.7−**630.2** K	
PBEsol, 700, 8, 0.60	1.227	521.7	609.3
soPBEsol, 700, 8, 0.60	1.076	591.8	626.3

bulk material and is evident already from the surprisingly strong overbinding of PBE. While it would certainly be interesting to see how an inclusion of non-local exchange and electron-correlation *via* TPT would change the picture, such a focused investigation of a single element is beyond the scope of this general work.

For Ba, the NBPs provided in the literature show a large variation of almost 17%. While the CRC Handbook, as well as the Tables for Physical and Chemical Constants, provide values of 2118−2173 K,[26,27] other sources provide a distinctly lower value of 1910−1950 K,[23–25] or even 1810 K in Holleman-Wiberg.[28] Zhang and coworkers suggested the value of 1910 K based on a prediction of their neural network of 1600 K. However, they have not considered ref. 28 in their study,[22] which provides a value much closer to their estimate. Based on the accurate prediction of the NBPs of Ca and Sr with a very systematic over-estimation of 3% with PBE, we conclude that this approach is as accurate for Ba, for which it affords an NBP of 1984 K (the influence of spin-orbit coupling is < 5 K). Correcting for the systematic deviation observed for Ca and Sr yields a value of ≈ 1920 K, which is in excellent agreement with refs. 23,24 and 25, but more than 6% and 8% away from 1810 K and >2100 K, respectively.

For the heavy metal Hg an accurate account of relativistic effects is essential for accurate properties. Here, the incremental nature of the approach not only enables the inclusion of computationally very demanding spin-orbit coupling (SOC), but also an in-depth analysis of their influence on the physicochemical properties, which we will demonstrate in the following. The gas phase of Hg consists of weakly interacting atoms with $\Theta = 1$. Spin-orbit relativistic (so)PBEsol provides a cohesive energy of -0.622 eV (rhombohedral phase), corresponding to a weak underbinding compared to the experiment, as evident from the λ of 1.076 (for a detailed discussion of the experimentally lowest structure, see ref. 48). In the scalar-relativistic (sr) approximation, while the structure largely remains the same, the calculated cohesive energy is distinctly smaller with -0.546 eV, resulting in a λ of 1.227. The so-relativistic calculation provides a NBP of 626.3 K in excellent agreement with the experimental value of 630.2 K. Conducting all calculations in the sr approximation and including SOC only *via* λ-scaling leads to a NBP of 609.3 K (521.7 K without scaling), and thus a slightly larger deviation from the experiment. This shows that here, SOC effects may be included *via* λ-scaling without loosing much accuracy. Note that SOC also has a significant impact on the volume, leading to a significant increase of the density from 11.6 g/ccm (sr) to 12.3 g/ccm (so). However, as already observed for K, the influence onto the calculated NBP is negligible with 0.1 K.

3.3 Liquid Entropies

In addition to calculating and comparing NBPs, the calculated liquid entropies may be compared directly to experimental ones.[39] For this, we obtain experimental entropies by linear interpolation between the four closest values provided in ref. 39 at the corrected effective temperature ($T_{\mathrm{cor}} = \lambda T_{\mathrm{sim}}$), and plot them against the calculated entropies in Fig. 3. Concerning the calculated values, we include the purely classical entropy S used for the linear extrapolation, as well as the sum of classical and electronic entropy $S + S_{\mathrm{el}}$. Inspection of Fig. 3 reveals a picture very consistent with that of the NBPs. In cases where the calculated NBP agrees well with the experimental data, also the entropies are in good agreement, which is perhaps most evident from the example of Mn. It is the element with the largest deviation of the calculated NBP between DFAs, which is reflected in the entropies. Similar to the NBP, SCAN shows a substantial deviation, while PBE agrees reasonably well. The other example with a notable deviation is Ba, and illustrates the disadvantage of a comparison to "experimental" entropies. The problem is that the entropy is not directly accessible experimentally, but modeled to reproduce various experimental data under certain assumptions, which may be flawed. The only source for the liquid entropy of Ba uses an NBP of 2119 K,[39] which is – as previously discussed – most certainly too high. This presumably explains why the deviation of the calculated entropies is more significant for Ba than for Ca and Sr. For all other elements for which experimental data is available (all except Xe), the agreement between calculated and experimental entropies is excellent. Statistical analysis of the shown

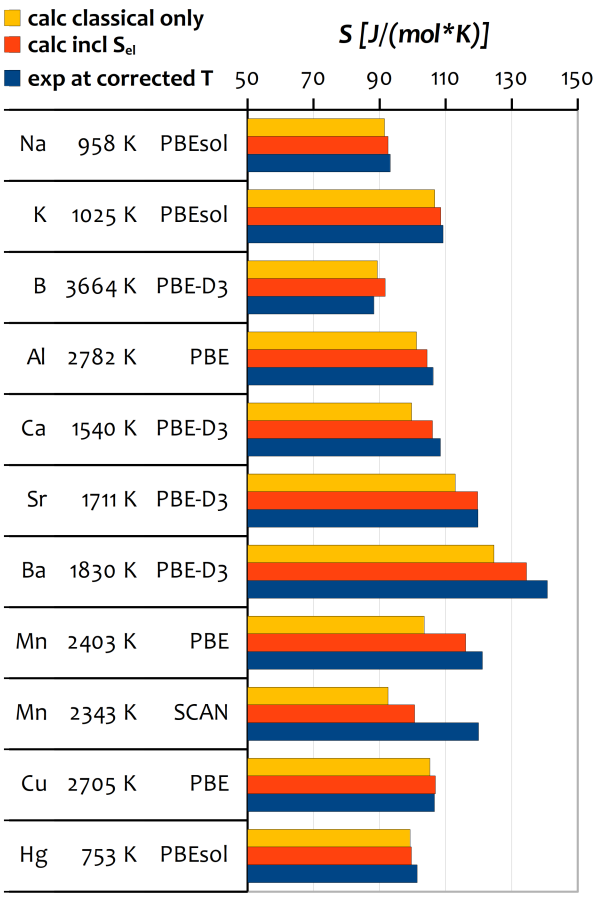

Fig. 3 Calculated liquid entropies excluding (yellow) and including (orange) the electronic entropy compared to experimental values for the corrected temperature (λT_{sim}, given on the x-axis, blue). All values given in J/(mol*K). Experimental values are obtained by linear interpolation between the four closest values from ref. 39.

data (one calculation per element, using PBE-D3 for Ca, Sr and Ba, PBEsol for K, and PBE for Mn) confirms that including the electronic entropy systematically improves the agreement with the experimental data for both temperatures. For the experimental value at the effective temperature, including S_{el} reduces the MD from -5.7 J/(K*mol) (-4.7%) to 1.1 J/(K*mol) (0.7%) and the MAD from 5.8 J/(K*mol) (4.9%) to 2.3 J/(K*mol) (2.0%). In conclusion, this comparison shows that the approach can also provide very accurate liquid entropies with a MD below 1%, and moreover, that their accuracy strongly correlates with that of the predicted NBPs.

4 Summary and Conclusion

We have presented and evaluated an approach for the prediction of normal boiling points (NBPs) and entropies of atomic liquids from first principles. The approach efficiently combines thermodynamic integration (TDI) from a non-interacting reference with thermodynamic perturbation theory (TPT) based on plane-wave DFT to provide numerically converged liquid Gibbs energies at reasonable computational cost. The incremental scheme not only allows the consideration of computationally demanding effects, like explicit spin-orbit coupling as demonstrated for Hg, but can moreover reveal the impact of each contributions on the NBP as well as other physicochemical properties. Such an analysis revealed that the electronic degeneracy and low-lying excited states of the atoms in the gas phase significantly affect the calculated NBPs, whereas conbtributions from two-body interactions — direct as well as indirect *via* dimer formation — are negligible for the studied elements.

Calculating the NBPs of a representative set of elements including insulators (Xe), semiconductors (B), alkaline (Na, K), alkaline-earth (Ca, Sr, Ba), transition (Cu, Mn, Hg) and main-group metals (Al), we demonstrated the approach to be robust with respect the choice of the density-functional approximation (DFA), and very accurate with an MAD $< 2.0\%$. The only significant deviation between tested DFAs was observed for Mn, which we traced back to the challenging electronic structure of the atom. For B and Ba, the variation between the literature values of the NBP is several times lager (9% and 17%) than the overall MAD of the calculated values. Most notably is Ba, where the deviation of the calculated NBPs is moreover very systematic for the lighter congeners. Accounting for this, our estimate of 1920 K is in excellent agreement with the literature value of 1910 K,[22–25] questioning the accuracy of other values of 1810 K and well above 2000 K reported elsewhere.[26–28]

The robustness of the calculated NBPs regarding the choice of the DFA is a result of λ-scaling. The fact that this works so well for the NBP of the studied elements can be rationalized by considering that for their liquid (and solid) to gas transitions, all interatomic forces have to be overcome. As a result, details of the potential shape (width, asymptotic behavior etc.) do not exert a large influence, whereas the total interaction strength reflected in the potential depth is crucial. Since λ scaling is based on the relation of the cohesive energies, it very efficiently corrects for the potential depth, such that various DFAs provide reasonably accurate NBPs. Interestingly, as we have learned form other ongoing projects, an entirely different pictures emerges for the melting point, which does strongly depend on the shape and particularly the width of the potential.[16] This will be explored in detail in forthcoming projects.

Besides the NBPs, also calculated liquid entropies were shown to be in excellent agreement with reference values,[39] while their accuracy correlated with that of the NBPs. The mean deviation (MD) from the references over all examples is just 2.0% or 1.1 J/(mol*K). Since the calculation of the NBPs requires the Gibbs energy of the gas phase, whose calculation becomes tedious if several low-lying electronic states and/or molecular species are present, this direct comparison of entropies expands the scope of systems for which the approach can be tested significantly.

One limitation of the presented approach in its current form is that it is only applicable to structurally simple systems that constitute a deep global minimum on the potential-energy surface, which essentially excludes molecular liquids. The underlying problem is that a presence of complex structure conflicts with the reversibility-criterion of the TDI, where covalent bonds are readily broken and reformed at low interacting strength. We are currently testing an approach which overcomes this limitation through a selective integration of the inter-molecular forces,

whereas intra-molecular forces are unaltered. This changes the reference to a gas of non-interacting molecules, whose intramolecular (vibrational, conformational) contributions can be separated out and calculated independently. To separate inter- and intramolecular forces, n additional gradient calculations are required at each simulation step, one for each of the n molecules or (more general) fragments in the simulation. Since each of the fragments much smaller than complete system, this is computationally cheap if atom-centered basis functions are used instead of plane-waves.

However, even in its current form, the approach is uniquely useful, *e.g.*, for predicting the aggregate states of short-lived super-heavy elements, to study the influence of periodic trends and relativistic effects on the boiling point, but also to study the performance of density-functional theory for the description of atomic liquids as well as their phase transitions.

5 Computational Details

All DFT calculations have been carried out with VASP 5.4.4.[49–52] The core region is modeled using the projector-augmented wave (PAW) approach of Joubert and Kresse using the softest potential available in the VASP library.[53,54] Calculations with the SCAN functional take into account non-spherical contributions from the PAW potentials (`LASPH = TRUE`) through TPT. The volume calculations were conducted in the Γ-point approximation, or, if there was a significant non-linear influence, with a 2^3k-point grid (B, Al and Cu). Thermodynamic integration was conducted with the lower energy cut-off shown in Tab. 4 in the Γ-point approximation, except for B and Hg, where a 2^3 grid was employed. Thermostating was done with a Nosé-Hoover thermostat with `SMASS = 2-4`, SCF convergence (`ECONV`) reduced to 10^{-4}, and `PREC = normal`. The timestep was chosen for each case based on atomic mass and simulation temperature, and further reduced if necessary to ensure accurate thermostating. For the integration point closest to the non-interacting limit, the timestep is reduced significantly to stabilize the simulation numerically. In few cases with particularly small λ values, it was required to switch to a Langevin thermostat with a very large friction coefficient (`LANGEVIN_GAMMA = 8+`). In general, each integration point was sampled with at least about 10000 steps, of which the first 2000 are considered equilibration. The length of each simulation was chosen such that the statistical error of the NBP is below 0.2%. For thermodynamic perturbation theory, several single-point calculations are conducted for 10-20 statistically independent snapshots taken from the trajectory with $\lambda = 1$; one with the same settings as the simulation, one with the increased cut-off, precision and convergence critera (`PREC = accurate`, `ECONV` = 10^{-6}), and finally one with all settings from above as well as a finer k-point grid as specified in Tab. 4. The contributions from these steps are shown for Xe, K and B in Tab. 1.

Conflicts of interest

There are no conflicts to declare.

Acknowledgements

JMM acknowledges financial support by the Alexander-von-Humboldt Foundation (Bonn) and the use of New Zealand eScience Infrastructure (NeSI) high performance computing facilities (nesi000474). JMM wants to thank S. Schmitz, A. Hansen, and S. Grimme (Bonn) for helpful comments on the manuscript. OS wants to thank P. Schwerdtfeger (Auckland) for helpful discussions regarding the scaling relation.

Notes and references

1 H. Gomez, M. Bures and A. Moure, *Philosophical Transactions of the Royal Society A: Mathematical, Physical and Engineering Sciences*, 2019, **377**, 20180203.
2 O. Sugino and R. Car, *Phys. Rev. Lett.*, 1995, **74**, 1823–1826.
3 A. D., M. J. Gillan and G. D. Price, *The Journal of Chemical Physics*, 2002, **116**, 6170–6177.
4 D. Alfè, L. Vočadlo, G. D. Price and M. J. M. J. Gillan, *J. Phys. Condens. Matter*, 2004, **16**, S973—-S982.
5 B. Grabowski, L. Ismer, T. Hickel and J. Neugebauer, *Phys. Rev. B*, 2009, **79**, 134106.
6 L.-F. Zhu, B. Grabowski and J. Neugebauer, *Phys. Rev. B*, 2017, **96**, 224202.
7 U. R. Pedersen, F. Hummel, G. Kresse, G. Kahl and C. Dellago, *Phys. Rev. B*, 2013, **88**, 094101.
8 H. Nakai and A. Ishikawa, *The Journal of Chemical Physics*, 2014, **141**, 174106.
9 A. V. Marenich, C. J. Cramer and D. G. Truhlar, *The Journal of Physical Chemistry B*, 2009, **113**, 6378–6396.
10 S. Hilal, S. Karickhoff and L. Carreira, *QSAR & Combinatorial Science*, 2003, **22**, 565–574.
11 P. Y. Chan, C. M. Tong and M. C. Durrant, *Journal of Molecular Graphics and Modelling*, 2011, **30**, 120 – 128.
12 M. R. Fissa, Y. Lahiouel, L. Khaouane and S. Hanini, *Journal of Molecular Graphics and Modelling*, 2019, **87**, 109 – 120.
13 K. JOBACK and R. REID, *Chemical Engineering Communications*, 1987, **57**, 233–243.
14 S. Alavi and D. L. Thompson, *Molecular Simulation*, 2006, **32**, 999–1015.
15 N. Gaston, *Advances in Physics: X*, 2018, **3**, 1401487.
16 J.-M. Mewes, O. R. Smits, G. Kresse and P. Schwerdtfeger, *Angewandte Chemie International Edition*, 2019, **58**, 17964–17968.
17 D. M. Eike and E. J. Maginn, *The Journal of Chemical Physics*, 2006, **124**, 164503.
18 Y. Zhang and E. J. Maginn, *The Journal of Chemical Physics*, 2012, **136**, 144116.
19 F. Dorner, Z. Sukurma, C. Dellago and G. Kresse, *Phys. Rev. Lett.*, 2018, **121**, 195701.
20 M. Rang and G. Kresse, *submitted*, 2019.
21 K. S. Pitzer, *J. Chem. Phys.*, 1975, **63**, 1032–1033.
22 Y. Zhang, J. R. G. Evans and S. Yang, *Journal of Chemical & Engineering Data*, 2011, **56**, 328–337.
23 J. G. Stark and H. G. Wallace, *Chemistry Data Book*, John Mur-

ray: London, 1982, reprint 1984, pp. 8–11, 50–51.
24 J. G. Speight, N. A. Lange and J. A. Dean, *Lange's Handbook of Chemistry, 16th ed.*, McGraw-Hill: New-York, 2005, pp. 1.18–1.62, 1.124–1.127, 1.280–1.298.
25 J. Emsley, *The Elements, 3rd ed.*, Clarendon Press: Oxford, 1998, pp. 1.18–1.62, 1.124–1.127, 1.280–1.298.
26 G. W. Kaye and T. H. Laby, *Tables of Physical and Chemical Constants, 16th ed.*, Longman: Harlow, 1995, pp. 212–214, 338–342.
27 W. M. Haynes, D. R. Lide and T. J. Bruno, *CRC Handbook of Chemistry and Physics: A Ready-reference Book of Chemical and Physical Data, 97th ed.*, CRC Press: Boca Raton, FL, 2016-2017, pp. 4–49.
28 A. F. Holleman and N. Wiberg, *Lehrbuch der Anorganischen Chemie*, de Gruyter, Berlin; New-York, 101st edn, 1995.
29 N. D. Mermin, *Phys. Rev.*, 1965, **137**, A1441–A1443.
30 J.-M. Mewes, P. Jerabek, O. R. Smits and P. Schwerdtfeger, *Angewandte Chemie International Edition*, 2019, **58**, 14260–14264.
31 O. R. Smits, P. Jerabek, E. Pahl and P. Schwerdtfeger, *Phys. Rev. B*, 2020, **101**, 104103.
32 J. P. Perdew, K. Burke and M. Ernzerhof, *Phys. Rev. Lett.*, 1996, **77**, 3865–3868.
33 J. P. Perdew, K. Burke and M. Ernzerhof, *Phys. Rev. Lett.*, 1997, **78**, 1396.
34 Y. Zhang and W. Yang, *Phys. Rev. Lett.*, 1998, **80**, 890–890.
35 S. Grimme, J. Antony, S. Ehrlich and H. Krieg, *J. Chem. Phys.*, 2010, **132**, 154104.
36 S. Grimme, S. Ehrlich and L. Goerigk, *Journal of Computational Chemistry*, 2011, **32**, 1456–1465.
37 P. Jerabek, O. Smits, E. Pahl and P. Schwerdtfeger, *Mol. Phys.*, 2018, **116**, 1–8.
38 L. Schimka, R. Gaudoin, J. c. v. Klimeš, M. Marsman and G. Kresse, *Phys. Rev. B*, 2013, **87**, 214102.
39 Malcom W. Chase, Jr., *J. Phys. Chem. Ref. Data, Monograph No. 9*, 1998.
40 M. Griffel, *The Journal of Chemical Physics*, 1953, **21**, 1908–1908.
41 F. Weinhold, *The Journal of Chemical Physics*, 1998, **109**, 367–372.
42 M. von Domaros, E. Perlt, J. Ingenmey, G. Marchelli and B. Kirchner, *SoftwareX*, 2018, **7**, 356 – 359.
43 B. Cowan, *Topics in Statistical Mechanics*, Imperial College Press, 2005, vol. 3.
44 M. J. van Setten, M. A. Uijttewaal, G. A. de Wijs and R. A. de Groot, *Journal of the American Chemical Society*, 2007, **129**, 2458–2465.
45 K. K. Verma, J. T. Bahns, A. R. Rajaei-Rizi, W. C. Stwalley and W. T. Zemke, *The Journal of Chemical Physics*, 1983, **78**, 3599–3613.
46 V. O. Kiohara, E. F. Carvalho, C. W. Paschoal, F. B. Machado and O. Roberto-Neto, *Chemical Physics Letters*, 2013, **568-569**, 42 – 48.
47 J. R. Lombardi and B. Davis, *Chemical Reviews*, 2002, **102**, 2431–2460.
48 K. G. Steenbergen, J.-M. Mewes, L. F. Pasteka, H. W. Gaggeler, G. Kresse, E. Pahl and P. Schwerdtfeger, *Phys. Chem. Chem. Phys.*, 2017, **19**, 32286–32295.
49 G. Kresse and J. Hafner, *Phys. Rev. B*, 1993, **47**, 558.
50 G. Kresse and J. Hafner, *Phys. Rev. B*, 1994, **49**, 14251.
51 G. Kresse and J. Furthmüller, *Phys. Rev. B*, 1996, **54**, 11169.
52 G. Kresse and J. Furthmüller, *Comp. Math. Sci.*, 1996, **6**, 15.
53 P. E. Blöchl, *Phys. Rev. B*, 1994, **50**, 17953.
54 G. Kresse and D. Joubert, *Phys. Rev. B*, 1999, **59**, 1758.
55 M. Reif, *Fundamentals of Statistical and Thermal Physics*, Waveland Press, New York, 2009.

6 Supporting Information

In addition to the information presented on the following pages, the spreadsheets (in open-document format) used to conduct all calculations starting from the raw data (simulation averages) to the final boiling points are available upon request from the corresponding author.

Table 4 Settings used for the DFT-MD calculations in the thermodynamic integration and perturbation theory in the form (TDI→TPT). The reduced timestep used in the simulations near the non-interaction limit is given in parenthesis.

element	cut-off	k-grid	timestep [fs]
Xe (165 K, 200 K)	$200 \rightarrow 400$	$\Gamma \rightarrow 2^3$	8 (4)
K (923, 1023, 1123 K)	$200 \rightarrow 400$	$\Gamma \rightarrow 3^3$	8 (1)
K (1000 K)	$250 \rightarrow 500$	$\Gamma \rightarrow 2^3$	4 (1)
Na (1000 K)	$250 \rightarrow 500$	$\Gamma \rightarrow 2^3$	4 (1)
B (4000 K)	$350 \rightarrow 600$	$2^3 \rightarrow 3^3$	1 (0.25)
Al (2800 K)	$400 \rightarrow 600$	$\Gamma \rightarrow 2^3$	2 (1)
Ca (1800 K, 2100 K)	$200 \rightarrow 400$	$\Gamma \rightarrow 2^3$	4 (1)
Sr (1800 K)	$200 \rightarrow 400$	$\Gamma \rightarrow 2^3$	4 (1, 0.5)
Ba (2000 K)	$200 \rightarrow 400$	$\Gamma \rightarrow 2^3$	5 (0.5)
Cu (2700 K, 3000 K)	$350 \rightarrow 600$	$\Gamma \rightarrow 2^3$	2 (1)
Mn (2400 K)	$300 \rightarrow 600$	$\Gamma \rightarrow 2^3$	2 (1)
Mn (3200 K)	$300 \rightarrow 600$	$\Gamma \rightarrow 2^3$	1.5 (0.3)
sr/so Hg (700 K)	$250 \rightarrow 500$	$2^3 \rightarrow 3^3$	12 (3)

6.1 Calculation of the Gibbs Energy of the Liquid

The Gibbs energy of the liquid is calculated through TDI from a non-interacting reference (ideal gas). For this purpose the difference of the internal energies is integrated along the coupling parameter λ

$$\Delta G_{0-1} = \int_0^1 d\lambda \, \langle U_1(\mathbf{R}) - U_0(\mathbf{R}) \rangle_\lambda \ , \tag{7}$$

which relates the liquid with U_1 to the ideal gas with U_0 at the same T and V by scaling the forces, and added to the Gibbs energy of the ideal gas at the liquid equibrium volume (eqs. 11 and 12). Since the kinetic energy part of U_1 and U_0 is identical it cancels, and the potential part vanishes at zero interaction stength (u_0), the value of the integrand is the average internal potential energy calculated at full interaction strength $\langle U_1^{\mathrm{pot}}(\mathbf{R}) \rangle$ for configurations $\mathbf{R}$ generated with reduced interaction strength (at the respective λ). This integral is evaluated using numerical quadrature in the form of a n-point Gauss-Lobatto rule, in principle requiring one NVT simulation for each λ. Although most of these simulations are straightforward, the ones very close to the ideal-gas limit ($\lambda \ll 0.01$ or $< 1\%$ of the DFT forces) are tedious, whereas the simulation for the end point $\lambda = 0$ is not possible with a PAW+DFT methodology. This is because close-encounters between the (almost) non-interacting atoms lead to singularity in the energy resulting in numerical instabilities in errors in the simulations, partly resulting from overlapping core-electrons. An approach to circumvent these issues was devised and implemented by Kresse and coworkers and will be used here with slight modifications.[19]

The approach is based on substituting λ in eq. (7) with $\lambda(x) = (\frac{x+1}{2})^{1/(1-\kappa)}$, which yields

$$\Delta G = \frac{1}{2(1-\kappa)} \int_{-1}^{1} f(\lambda(x)) \lambda(x)^\kappa dx \, . \tag{8}$$

This introduces an explicit dependency on λ in the integrand, which not only dampens the impact of the technically challenging calculations near the non-interacting limit (*cf.* effective weights in Fig. 4), but also completely eliminates the point for $\lambda = 0$. This is because the substitution introduces a parameter κ, which fulfils another role: It guides the mapping of the quadrature points between the domains. While a value close to 0 retains the original (equidistant) spacing of the Gauss-Lobatto quadrature, choosing κ close to 1 increases the density of quadrature points in the λ domain in the region close to $\lambda = 0$, where the slope of $f(\lambda)$ is the largest (*cf.* Fig. 4). While Kresse and coworkers suggest $\kappa > 0.8$, we demonstrate here that at least for the calculation of NBPs, much smaller values suffice. This dramatically reduces the computational effort as it allows to avoid the technically challenging simulations near the non-interacting limit almost entirely.

Since it is nevertheless prohibitively expensive to carry out the TDI at a converged level of theory, it is instead combined with thermodynamic perturbation theory (TPT)

$$\Delta G_{1-2} = -\frac{1}{\beta} \ln \langle e^{-\beta [U_2(\mathbf{R}) - U_1(\mathbf{R})]} \rangle_1 \ , \tag{9}$$

where the index after the angle bracket indicates that the difference ΔU_{1-2} is evaluated for configurations generated by H_1. Thus, by exploiting the linear shift of a refined Hamiltonian (*e.g.* increased cut-off, k-points or even another functional), TPT can often provide a very good estimate for the respective Gibbs-energy difference from as few as 5-20 single-point calculations. Instead of the exact equation, we use the second-order cumulant expansion

$$\Delta G_{1-2} \approx \langle \Delta U \rangle_1 - \frac{\beta}{2} \langle (\Delta U - \langle \Delta U \rangle)^2 \rangle_1 \ , \tag{10}$$

which is sufficiently accurate since already the second-order term is $\ll 1$ meV/atom in all cases, and can thus be neglected. Using TPT, all final results are converged to within ≈ 2 meV/atom, which translates into a error in the NBP of about 2 K.

6.2 Calculation of the Gibbs Energy of the Gas Phase

The Gibbs energy of the gas phase is calculated for the non-interacting (ideal) gas at its equilibrium volume and ambient pressure. For a given atomic degeneracy Θ, volume V, temperature T, particle number N and mass m this is

$$G^{\mathrm{id}} = F^{\mathrm{id}} + pV = -k_B T \ln(Z(\Theta, T, V, N)) + pV, \text{ with} \tag{11}$$

$$Z(T,V,N) = \frac{(\Theta V)^N}{\Lambda^{3N} N!} \text{ and } \Lambda = h\sqrt{\frac{\beta}{2\pi m}} \quad . \tag{12}$$

For the gas phase, this equation is solved using the Stirling approximation, which is sufficiently accurate since we are considering an arbitrary number of particles. The same equation is also used to calculate the Gibbs energy of the non-interacting refer-

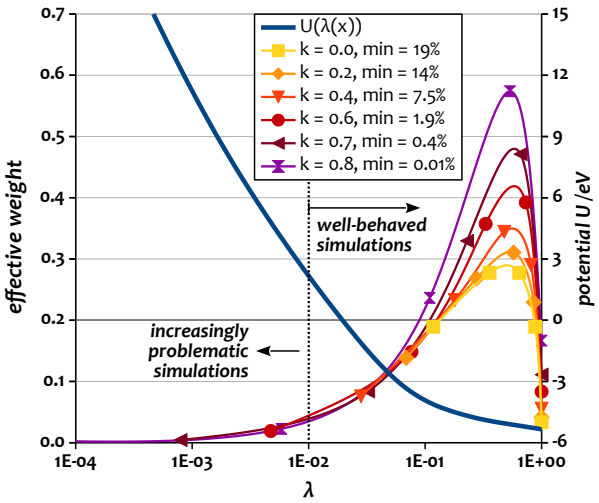

Fig. 4 Effective weight plotted against the λs (logarithmic scale) at which simulations have to be conducted for a 6-point Gauss-Lobatto rule for several different choices of κ. The interaction-strength for the most "non-interacting" simulation (min) is given in the legend in %. For reference, the evolution of the value of the integrand taken from B at 4000 K with PBE-D3 is shown in blue on the secondary axis. The effective weight is $(w_i\lambda^\kappa)/(2(1-\kappa))$ where w_i is the weight from the respective Gauss-Lobatto rule.

ence for the liquid (at the equilibrium volume of the liquid). Here, however, the Stirling approximation is no longer suitable since the number of particles is finite (61 or 64), and the pV term is negligible. Moreover, since – in contrast to the real atoms in the gas phase – the non-interacting reference for the liquid consists of hypothetical point-masses, they are not degenerate.

To validate the accuracy of the non-interacting model, we evaluate the first virial (two-body) correction for each of the examples assuming a Lennard-Jones (12,6) potential with the parameters derived from first-principles calculations for the respective dimers. This leads to the following integral

$$G^g_{\mathrm{LJ}} = G^g_{\mathrm{id}} - \frac{2\pi N^2}{V\beta}\int\left[r^2 e^{-4\varepsilon\beta\left[\left(\frac{\sigma}{r}\right)^{12}-\left(\frac{\sigma}{r}\right)^{6}\right]}-1\right]dr \qquad (13)$$

which can be evaluated as described in ref. 43. This provides generally very small corrections (≤ 1.0 meV/atom), which in turn have a negligible impact on the calculated boiling points (≤ 1 K).

7 Determination of Equilibrium Volumes

To calculate the equilibrium volume, the 61 or 64-atom supercells are simulated with the default settings (*cf.* Tab. 4) at several slightly different volumes until the statistical average of the pressure is converged to within 0.3 kBar. For about 5-20 equidistant snapshots from the trajectory, single-point calculations are conducted with the converged settings to obtain a correction for the influence of Pulay stress, a finer k-point grid, and increased numerical precision (as well as spin-orbit coupling in case of Ba and Hg). The corrected pressures at each point are fitted with a second-order polynomial and interpolated to the x-intersection ($p = 0$, note that using p=0.001 kBar consistent with ambient pressure would provide virtually identical volumes). Final volumes are confirmed during the TDI, where the simulation with $\lambda = 1$ and subsequent TPT provides the residual pressures given in Tab. 5, along with the calculated atomic volumes and corresponding densities.

Table 5 Calculated equilibrium volumes (in Å^3/atom), corresponding densities ρ (in g/cm^3), and residual pressures (in kBar) for all studied elements. Volumes of Al, Cu, B, and Cn are calculated with 2^3k-point grid in the simulations, all others employ the Γ-point approximation and include the effect of more k-points perturbatively.

element/DFA/T_{sim}	V/atom	ρ	residual p
Xe/PBE-D3/165 K	79.8	2.73	0.1
Xe/PBE-D3/200 K	85.8	2.54	0.1
Xe/revPBE-D3/165 K	79.8	2.73	−0.1
K/PBE-D3/1000 K	90.42	0.718	0.0
K/PBEsol/1000 K	93.22	0.696	0.3
K/PBE/1000 K	101.9	0.637	0.1
B/PBE-D3/4000 K	8.820	2.04	−0.2
Al/PBE/2800 K	23.62	1.90	0.1
Na/PBEsol/1000 K	46.24	0.825	0.2
Ca/PBE/1800 K	52.51	1.27	−0.5
Ca/PBED3/1800 K	47.63	1.40	0.2
Ca/PBEsol/1800 K	49.22	1.35	−0.2
Sr/PBE/1570 K	66.92	2.17	0.0
Sr/PBED3/1800 K	64.00	2.27	−0.2
Sr/PBEsol/1800 K	65.55	2.22	−0.7
Ba/PBE/2000 K	81.25	2.81	0.0
Ba/PBED3/2000 K	73.40	3.11	0.1
Mn/PBE/3200 K	12.75	7.16	0.5
Mn/RPBE/2400 K	12.49	7.30	−0.4
Mn/SCAN/2400 K	11.58	7.89	−1.2
Cu/PBE/2400 K	12.49	7.30	−0.4
Hg/soPBEsol/700 K	25.86	12.9	−0.1

7.1 Derivation of the Scaling-Relation of the Gibbs Energy

The following derivations built on those presented to ref. 16, which demonstrates that for any atomic system in the classical Born-Oppenheimer picture, a scaling of the interatomic potential ϕ with a factor λ, phase-transition temperatures scale with the same factor. Although ref. 16 explicitly includes the boiling points, we will show in the following that the simple transition-temperature scaling is incorrect for the BP. Instead, the corrected BP, or in other words the BP for a scaled interaction potential $\lambda\phi$, has to be determined from the intersect of corrected (scaled) Gibbs energy for the liquid with the (unaffected) Gibbs energy of the gas. For this purpose, we go beyond the derivations presented in ref. 16 and provide an analytical expression for the absolute Gibbs energies of the solid and liquid phase as a function of a linear scaling of the potential.

Let us begin with the description of the Gibbs energy for the solid and liquid phase. In ref. 16 it is shown that

$$U(\lambda T, \lambda\phi) = \lambda U(T,\phi)\,. \qquad (14)$$

However, no such relation was derived for the absolute entropy, but only for the relative melting entropy ΔS^{s-l}. While this is sufficient to derive the transition-temperature scaling for the MP, it was insufficient to calculate the change in the absolute Gibbs en-

ergy upon scaling the potential.

To derive an analytical relation also for S, let us consider a simple solid and liquid. At sufficient high temperatures, such that classical mechanics is applicable, it follows from the equipartition theorem that the total mean energy, the sum of kinetic and potential energy, is proportional to the temperature.[55] Hence, the term p^2 in the kinetic part to the general expression for the entropy scales linearly with T,

$$S(T,\phi) = \frac{U}{T} + k_B \ln Z \tag{15}$$

$$= \frac{U}{T} + k_B \ln\left(\int e^{-\phi(r)/k_B T} dr + \int e^{-p^2/2mk_B T} dp \right) \tag{16}$$

$$S(\lambda T,\lambda\phi) = \frac{\lambda U}{\lambda T} + k_B \ln\left(\int e^{-\lambda\phi(r)/k_B \lambda T} dr + \int e^{-\lambda p^2/2mk_B \lambda T} dp \right), \tag{17}$$

such that as evident from the last line, the λs cancel out. This is because the accessible configuration space remains exactly the same when potential depth ϕ and available kinetic energy T are multiplied by the same factor λ. This concludes that for both the solid and the liquid phases the entropy is unaffected by the scaling and thus

$$S(\lambda T,\lambda\phi) = S(T,\phi)\,. \tag{18}$$

Accordingly, the respective Gibbs energy (assuming $pV = 0$) becomes

$$G(\lambda T,\lambda\phi) = U(\lambda T,\lambda\phi) - \lambda T S(\lambda T,\lambda\phi) \tag{19}$$

$$= \lambda U(T,\phi) - \lambda T S(T,\phi) \tag{20}$$

$$= \lambda G(T,\phi)\,, \tag{21}$$

showing that the Gibbs energy of the condensed phases is linear with respect to a simultaneous scaling of T and ϕ. This proves eq. (3-5) in the manuscript, and provides the means to correct the Gibbs energy. It should be pointed out that this holds for any temperature sufficiently high to consider the system in the classical picture, which thus certainly including the boiling and melting points of most elements.

Let us now move to the ideal gas and rationalize why it behaves different, or, in other words, why it does not scale like the solid and liquid. Using Stirling's approximation, $\ln N! = N\ln N - N$, the Helmholtz energy of the ideal gas takes the form

$$F^{id} = -k_B T \ln Z \tag{22}$$

$$= -Nk_B T \ln\left[\left(\frac{mk_B T}{2\pi\hbar^2} \right)^{3/2} \frac{V}{N} \right] - kT_B N \tag{23}$$

The partial derivatives

$$S = \left.\frac{\partial F}{\partial T}\right|_{V,N} = -k_B T \left.\frac{\ln Z}{\partial T}\right|_{V,N} \tag{24}$$

$$p = \left.\frac{\partial F}{\partial V}\right|_{T,N} \tag{25}$$

are used to obtain expressions for the entropy and pressure

$$S = Nk_B \left(\frac{5}{2} + \ln\left[\left(\frac{mk_B T}{2\pi\hbar^2} \right)^{3/2} \frac{V}{N} \right] \right) \tag{26}$$

$$pV = Nk_B T \tag{27}$$

since $U = F + TS$, we have

$$U = k_B T^2 \left.\frac{\ln Z}{\partial T}\right|_{V,N} \tag{28}$$

$$= \frac{3}{2} Nk_B T\,. \tag{29}$$

and because $G = F + pV$

$$G = -Nk_B T \ln\left[\left(\frac{mk_B T}{2\pi\hbar^2} \right)^{3/2} \frac{V}{N} \right]. \tag{30}$$

Upon scaling of the temperature (and potential) with λ, a new term shows up in the Gibbs energy of the ideal gas

$$G(\lambda T) = -Nk_B \lambda T \ln\left[(\lambda T)^{5/2} \left(\frac{mk_B}{2\pi\hbar^2} \right)^{3/2} \frac{k_B}{P} \right] \tag{31}$$

$$= Nk_B \lambda T \ln\left[T^{5/2} \left(\frac{mk_B}{2\pi\hbar^2} \right)^{3/2} \frac{k_B}{P} \right] + Nk\lambda T \ln[\lambda^{5/2}] \tag{32}$$

$$= \lambda F(T) + Nk_B \lambda T \ln[\lambda^{5/2}]\,. \tag{33}$$

Since the ideal gas is – in constrast to the condensed phases – independent on the interaction potential, the above derived relation merely show the temperature-dependence of the Gibbs energy of the gas. Unsurprisingly, $G^g(T)$ is not linear in T, and as a consequence, the simple scaling of the BP is not possible. However, as evident from eqs. (21-23), the entire Gibbs energy curve for the liquid phase can be corrected for linear changes in the potential, and the corrected BP extracted as the intersect between the corrected Gibbs energy of the liquid $G^l(T,\lambda\phi)$ and the unaltered Gibbs energy of the gas phase $G^g(T)$.

Table 6 Calculated Gibbs energies, internal energies (in eV/atom), as well as classical and electronic entropies (in meV/[atom*K]) for the liquid phase of all studied elements.

DFA, T_{sim}, T_{eff}	G	U	S	S_{el}
Xenon				
PBE-D3, 165, 165	−0.2368	−0.1406	0.5831	0.0
Sodium				
PBEsol, 1000, 959	−1.8091	−0.8605	0.9486	0.0112
Potassium				
PBE, 1000, 1073	−1.6822	−0.5685	1.1137	0.0200
PBE-D3, 1000, 945	−1.7617	−0.6803	1.0822	0.0182
PBEsol, 1000, 1002	−1.7311	−0.6371	1.0940	0.0188
Boron				
PBE-D3, 4000, 3664	−8.5304	−4.8373	0.9233	0.0248
Aluminum				
PBE, 2800, 2782	−5.5099	−2.5913	1.0488	0.0327
Calcium				
PBE, 1800, 1729	−3.2486	−1.3322	1.0644	0.0658
PBE-D3, 1800, 1540	−3.4238	−1.5414	1.0327	0.0657
PBEsol, 1800, 1568	−3.4256	−1.5298	1.0458	0.0656
PBEsol, 2100, 1829	−3.7680	−1.4770	1.0909	0.0755
Strontium				
PBE, 1570, 1680	−2.9156	−1.1088	1.1509	0.0621
PBE-D3, 1800, 1712	−3.3560	−1.2506	1.1697	0.0707
PBEsol, 1800, 1714	−3.3618	−1.2305	1.1841	0.0708
Barium				
PBE, 2000, 2026	−3.9186	−1.2899	1.3144	0.1088
PBE-D3, 2000, 1830	−4.0781	−1.4942	1.2920	0.1020
Manganese				
PBE, 3200, 2402	−6.3447	−2.9140	1.0721	0.1307
RPBE, 2400, 2198	−4.7648	−2.3975	0.9852	0.0987
SCAN, 2400, 2342	−4.4795	−2.1522	0.9697	0.0833
Copper				
PBE, 2700, 2705	−5.5273	−2.5896	1.0881	0.0175
PBE, 3000, 3006	−5.8769	−2.5039	1.1243	0.0220
Mercury				
soPBEsol, 700, 753	−1.0814	−0.3609	1.0279	0.0045